WARMINGUP

Innovatief Duurzaam Warmtecollectief

Dark Fibre for shallow subsurface characterization in urban environments

door

Auteurs: E. Obando Hernandez, S. Jansen, P. Doornenbal

15 juni 2022

Dark Fibre for shallow subsurface characterization in urban environments

Auteurs: E. Obando Hernandez, S. Jansen, P. Doornenbal
15 juni 2022

Dit project is uitgevoerd als onderdeel van het Innovatieplan WarmingUP. Dit is mede mogelijk gemaakt door subsidie van de Rijksdienst voor Ondernemend Nederland (RVO) in het kader van de subsidieregeling Meerjarige Missiegedreven Innovatie Programma's (MMIP), bij RVO bekend onder projectnummer TEUE819001.
WarmingUP geeft invulling aan MMIP-4 – Duurzame warmte en koude in gebouwde omgeving en levert daarmee een bijdrage aan Missie B – Een CO_2-vrije gebouwde omgeving in 2050.

Projectnummer
11205157

Keywords
Dark Fibre
MASW
Vs profile
Vs30

Jaar van publicatie
2022

Meer informatie
Edwin Obando Hernandez
T 06 15280865
E Edwin.obandohernandez@deltares.nl

Content

Summary

The WarmingUP4B project aims at developing low-cost monitoring techniques for induced seismicity and associated environmental effects related to production wells. To assess the potential effect of induced seismicity, it is of crucial importance to characterize the stiffness distribution in depth of the subsurface in terms S-wave velocity. S-wave surveys in geothermal environments requires the subsurface characterization from several hundred until few thousands of kilometres.

Recently, the use of fibre optics has enabled the possibility of using the already existing fibre optic telecommunication cables as seismic sensors. Among those massive telecommunication networks, there are thousands of kilometres of spare fibres also known as dark fibre, that offers the possibility of using thousands of points sensors in urban environments which are almost not reachable by standard survey systems. Nowadays, there is an enormous interest in understanding the real potential of dark fibre to characterize the subsurface in induced seismicity areas and particularly in highly populated areas.

In this report we present the results of a small-scale dark fibre array, aimed at assessing the potential a 90 m dark fibre array at Deltares campus, in Delft, for shallow S-wave velocity profiling in urban environments. We also discuss the potential of dark fibre for P-wave surveys. The results obtained with dark fibre are validated by deploying standard geophone arrays for both body and surface wave surveys. During 2 weeks of measurements we performed continuous recording of ambient/traffic noise generated by the running traffic nearby. The recorded noise data was cross-correlated utilizing seismic interferometric processing to compute virtual shot-gathers of 1.0-hour time segment. The computed virtual shotgathers showed coherent phase velocity spectrum utilized to compute S-wave velocity profiles at a maximum depth of 30 m. The dark fibre results appear to be comparable to S-wave velocity profiles retrieved using standard 1.0 Hz and 4.5 Hz geophones. The velocity transitions in depth, observed with all S-wave inverted profiles, appears to be similar to the transitions depicted by the P-wave tomography obtained with the standard refraction seismic tomography using 10 Hz geophones.

Cross-correlation of dark fibre noise data also provided information of P-wave arrivals in some cases comparable to standard P-wave arrivals observed in typical 10 Hz geophones generated by active sledgehammer impacts. Although, the similarities observed indicated the potential of the dark fibre, a more advanced processing and probably longer measuring time could provide better results. Likewise, the dark fibre was utilized for recording sledgehammer impacts (localized at the middle of the array) like an active refraction seismic survey. The apparent P-wave velocity depicted similar values to the ones determined via refraction seismic tomography at the test site. The active DAS shotgathers also showed clear and coherent dispersion pattern like the ones determined with 4.5 Hz geophones.

The processing scheme utilized in this study can be also implemented in large aperture arrays to successfully retrieve S-wave velocity profile in kilometre scale. This would be especially beneficial in urban environments where existing dark fibre could be an alternative to standard systems which are restrictive due to lack of available space.

1 Introduction

The WarmingUp4B project focuses on the development of low-cost monitoring techniques for induced seismicity and associated environmental effects. A crucial parameter to properly address the effect of induced seismicity is the 1D and/or 2D subsurface velocity characterization in terms of S-wave profiles. S-wave profiles are typically determined using either a single or an array of seismic sensors placed at the free surface, often limited to open space available to place the sensors. The DAS (Distributed Acoustic Sensing) technology that uses fiber optic cables as seismic sensors has emerged as an useful alternative for geophysical surveying and monitoring with unprecedented high spatial resolution and at a potentially lower cost (Daley et al., 2013; Tribaldos et al., 2019). Recent developments of DAS have also demonstrated a great potential, not only for velocity structure characterization, but also for monitoring of induced seismicity related to geothermal production (Lellouch, Spica, Biondi, & Ellsworth, 2019). Existing massive fiber optics telecommunication networks containing hundreds of kilometres of abandoned/spare fibres, also known as Dark Fiber, are available almost everywhere and can be potentially used as a massive seismic network to several environmental and engineering applications. Thus, dark fibre networks offer the possibility of characterizing the subsurface through ambient noise recordings (Ajo-Franklin et al., 2019; Dou et al., 2017; Tribaldos et al., 2019) even within highly populated areas where standard seismic surveying is rather difficult to implement.

In this project, we want to address the potential of Dark Fiber as a tool for evaluating the shallow subsurface composition using both, surface and body wave types derived from seismic interometry analysis. The results obtained from Dark Fiber data could contribute to improve the resolution of the shallow layering of existing Vs/Vp models for example at Groningen (Kruiver et al., 2017) area which will have a positive impact in the assessment of the environmental impact of induced seismicity e.g. seismic site response caused by geothermal activity.

1.1 Scope and objectives

The scope of the work is to assess the feasibility of Dark Fiber as a seismic sensor by using ambient noise for shallow ground characterization in terms of Vs at the first 30 m depth ($0 < Z < 30$m). The computed S-wave velocity profile would be used to better define the shallow layers which dominate the local ground response due to induced seismicity during geothermal activity. We also briefly address the potential of dark fibre for determining P-wave velocity using retrieved first breaks from high frequency traffic noise. The processing scheme utilized in this project would be later utilized for deeper surveys using a kilometre scale array.

In order to accomplish the main objective of this work, the following specific objectives are:

a) To determine the reliability of Dark Fibre to retrieve surface waves via cross-correlation using the background traffic noise nearby.
b) To assess the reliability of Dark fibre to properly capture the dispersion characteristics of the ground with respect to the one computed with standard geophones.
c) To evaluate the similarities of the computed S-wave velocity profile from Dark Fibre with respect to standard geophones at a maximum minimum depth of 30 m.
d) To evaluate the potential of Dark fibre to retrieve P-wave first arrivals.

2 Methods

2.1 Seismic interferometry

The seismic interometry method has become a very popular tool to construct active-like MASW shot-gathers utilizing low frequency passive seismic noise (Dou et al., 2017; Tribaldos et al., 2019). The method consists of performing cross-correlation of a pair of signals containing a diffuse wavefield which successfully retrieves the Green's function (Bensen et al., 2007; Wapenaar & Fokkema, 2006).

Initially, the raw data are pre-processed to remove mean and trend along a selected time time-window. Then each trace is time and frequency domain normalized. The selected long duration traces are split into short-time duration sub-windows (e.g. 30 s or 60 s). The short duration windows are cross-correlated and later averaged to enhance the signal to noise ratio to the retrieved virtual shotgather. An example of a pair of noise signals is displayed in Figure 2.1a plotted together with a cross-correlation function (CCF) Figure 2.1b. In a S-wave survey a large number of noise signals organized in a linear array allows depicting active like shotgathers containing surface waves energy.

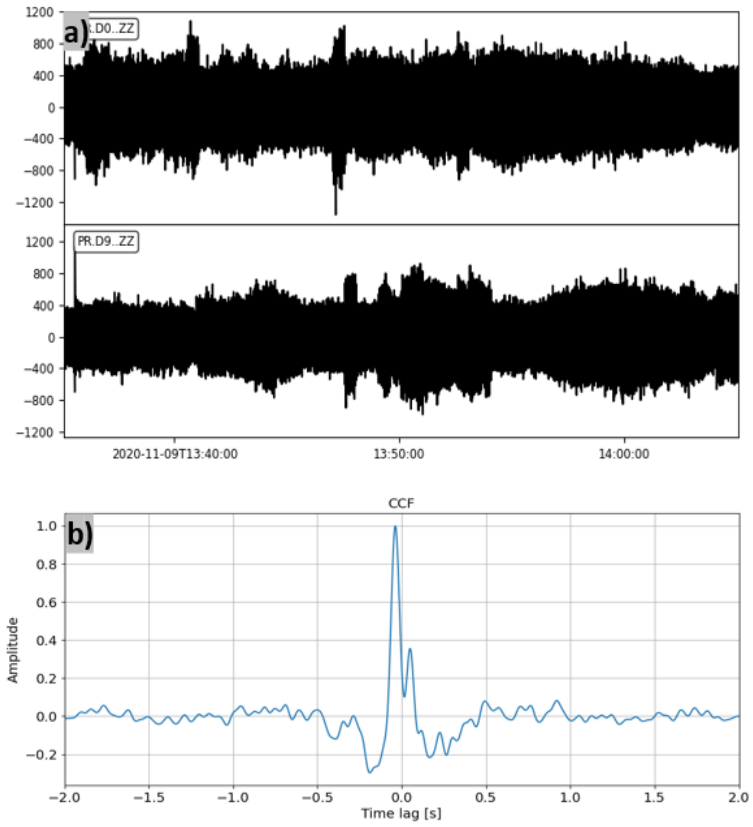

Figure 2.1. a) pair of noise records, and b) average cross-correlated trace (virtual trace) using 2.0 s as time shift (the one required to cross-correlate a pair a signals).

2.2 Multichannel Analysis of Surface Waves -- MASW

The method used for shear wave velocity computation is the multichannel analysis of surface waves method (MASW). The method was initially proposed for the determination of the shear wave velocity layering of the crustal structure for seismological applications (Gabriels, Snieder, & Nolet, 1987; McMechan & Yedlin, 1981) and later popularized for engineering applications (C. B. Park, Miller, & Xia, 1999). A complete description of the theoretical formulation and applications of the method are available in the literature (Garofalo et al., 2016; C. Park, Miller, Rydén, Xia, & Ivanov, 2005; C. B. Park & Miller, 2008).

The resulting phase velocity spectrum (dispersion image) from the MASW (Multichannel Analysis of Surfaces Waves) wavefield transformation method provides phase velocity distribution as function of frequency. An example of a phase velocity spectrum using the MASW method is displayed in Figure 2.2.

Figure 2.2a shows a typical example (synthetic record) of an active shotgather using a linear receiver spread and an impulsive source that generates body waves and surface waves. The dispersive surface waves are utilized to compute the phase velocity spectrum along a defined phase velocity and frequency interval (Figure 2.2b). The measured dispersion curve is obtained from the peak values of the phase velocity spectrum delineated by the dark red colour pattern.

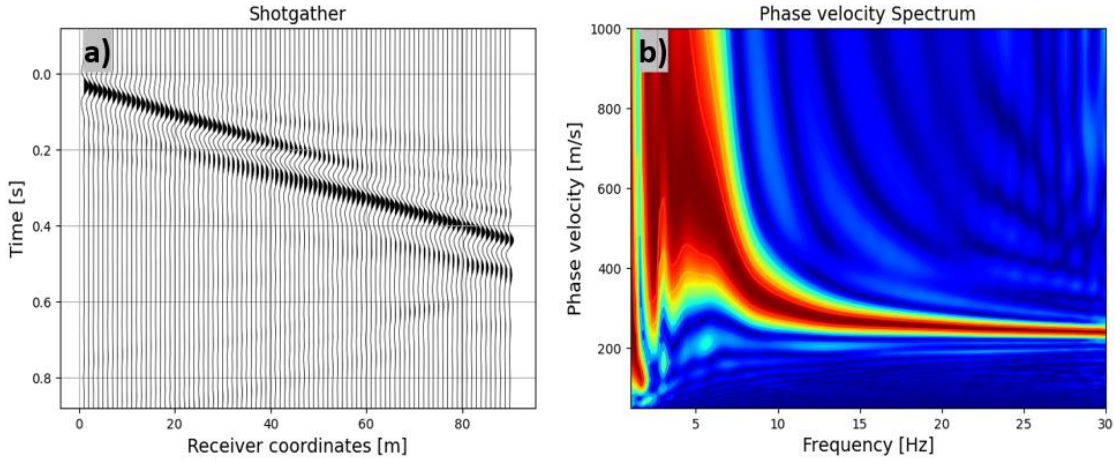

Figure 2.2. a) Typical MASW shotgather (synthetic waveforms) containing energetic surface waves, and b) computed phase velocity spectrum (used to extract the dispersion curve that is required for inversion). Red color is the highest energy (blue color is the lowest) from which the dispersion curve is extracted.

The interpretation of the extracted measured dispersion curve is focused on determining the maximum and minimum wavelength to be realistically resolved. The wavelength is defined as the ratio between phase velocity and frequency. The high frequency limits (short wavelength) provides information on the shallowest layer thickness to be resolved, while the low frequency limit (long wavelengths) defines the maximum depth of exploration.

2.3 Depth coverage and resolution

The inversion process consists of searching the velocity S-wave profile with depth whose forward response fits the measured dispersion curve computed from the maximum values of the phase velocity spectrum displayed in Figure 2.2b. The inversion allows determining the layer and velocity configuration with the lowest possible misfit.

Surface wave inversion is a non-linear process, which often leads to non-uniqueness problems, which means that several velocity profiles may provide an equally good fitting to the measured dispersion curve. Therefore, a rigorous analysis requires that the solution considers the statistical variability of the computed model (Foti et al., 2018; Sambridge, 1999a, 1999b; Wathelet, 2008).

A detailed description of advantages and disadvantages available of surface wave inversion methods can be found in the literature (Foti et al., 2018). A summary on the recommended acquisition geometry in relation of the target minimum and maximum exploration depth is provided in Table 2.1.

Table 2.1. Suggested parameters for active MASW analysis (Foti et al., 2018).

Parameter	Notation	Suggested values	Theoretical implications
Geophone spacing	dx	1.0 - 4.0 m	Aliasing --- usually minimum measurable wavelength $\lambda_{min} \sim 2dx$. Minimum near-surface layer thickness resolved depth Hmin ~ λ_{min} /3 to λ_{min} /2.
Array length	L	23 - 96 m	Maximum wavelength $\lambda_{max} \sim L$. Expected maximum depth of investigation λ_{max} /3 to λ_{max} /2.
Number of geophones	N	24 or 48	Quality of the dispersion image
Offset between source and first geophone	X_1	5 - 20 m	Near field and far field effect. Multiple shot locations strongly recommended.
Sampling interval	dt	0.5ms	Nyquist/Shannon frequency $f_{max} = \frac{1}{2dt} = 1000\ Hz$. Picking first arrivals (for refraction analysis).
Sampling frequency [Hz]	f_s = 1/dt	2000 Hz	Nyquist/Shannon frequency $f_{max} = \frac{1}{2dt} = 1000\ Hz$.
Post-trigger recording length [Time window]	T	2s	Record the whole surface wave train
Pre-trigger recording length		0.1 – 0.2s	Mitigating leakage during processing

In practice the suggested values, displayed in Table 2.1, such as number of receivers and sampling frequency are selected depending on the target maximum exploration depth and resolution. It is always desirable to use a short receiver separation (dx=2 m or less) and a spread length of at least 3 times the maximum target depth. Receiver separation larger than 2.0 m and a reduced number of receivers, induce spatial aliasing problems, and reduces the resolution of the final profile. For a standard active MASW survey a sampling frequency of 1000 Hz is enough to accurately retrieve broadband (low and high frequencies) surface waves. Higher sampling frequencies are necessary only if additional information such as the first arrivals (from P-wave) would be necessary to constrain the inversion process. Additional first arrivals are also useful at sites with complex soil configuration and where the uncertainty of the inverted S-wave inversion is high.

3 Field survey

3.1 Survey geometry

The survey site is localized in Delft campus of Deltares. The field set-up implemented in this project is displayed in Figure 3.1. The L-shape dark fibre cable available for the DAS measurements is extended along 240 m, delineated by the dark red colour line. The segment selected is located along the Geohal facility where 3 geophone spreads are placed alongside each other with an approximate length of 90 m (Figure 3.2).

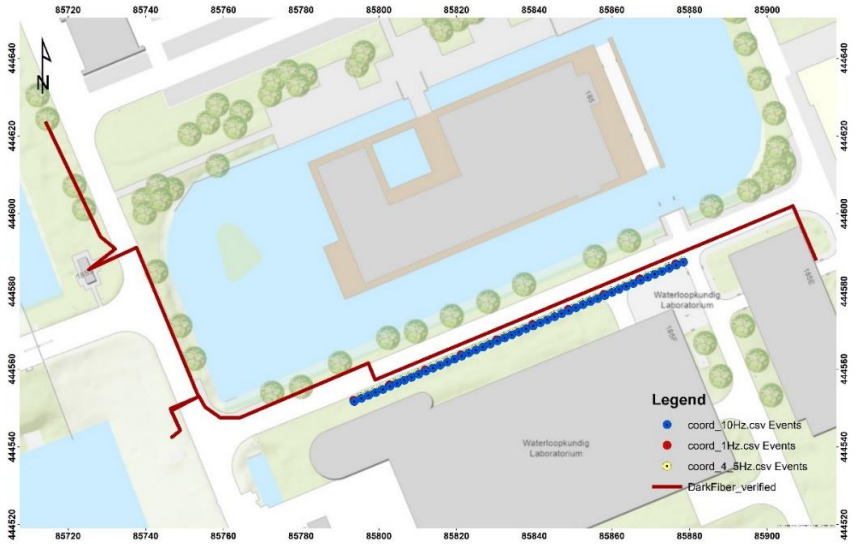

Figure 3.1 Geometry of Dark Fibre and Geophone spreads utilized for the measurements, together with the 1.0 Hz (10), 4.5 Hz (47), and 10.0Hz (47) vertical component geophones.

Figure 3.2 a) 1.0 Hz geophones spread (each piece inside a plastic bag) spaced at 10.0 m, and b) 4.5 Hz (yellow color) and 10.0 Hz (blue color) vertical geophones spaced at 2.0 m.

The field geometry adopted per system (4.5Hz, 10.0Hz and 1.0Hz geophone spreads) is summarized in Table 3.1. Notice that for surface wave survey we used 1.0 kHz sampling frequency, enough to map surface waves energy, while for body waves we used a sampling frequency of 8.0 kHz to enhance the higher frequency P-wave arrivals recorded with 10 Hz receivers.

Table 3.1 Acquisition geometry per system.

System	dx (m)	Fs (kHz)	N (Number of traces/channels)	L (m)
4.5 Hz	2.0	1.0	47	92
10.0 Hz	2.0	1.0 (8.0 for Refraction Seismic)	47	92
1.0 Hz	10.0	1.0	10	90

Notice that the existing obstacles at the site did not allow placing the geophone spread at the exact position of the straight dark fibre segment. Thus, the selected fibre optic segment will be about 7.0 meters off the geophone lines. In Figure 3.3 the red stars represent the selected shot positions to retrieve body and surface waves with both 4.5 Hz and 10.0 Hz geophone spreads.

The minimum and maximum depth of investigation resolved in the inversion process is determined by the minimum and maximum wavelength observed. Thus, based on the resolution and survey depth required, we use 47, 4.5 Hz and 10, 1 Hz receivers placed in a linear array with 2.0 m and 10 m separation, respectively. This approximately corresponds to a maximum depth of exploration of around 30 m. The 2.0 m spacing of the 4.5 Hz geophones allows a minimum wavelength of 4 m (2*dx), which corresponds to a minimum resolvable exploration depth of 1.33 m. The iDAS interrogator with a gauge length of 10 m allows retrieving a minimum wavelength of 15 m and a maximum wavelength of 90 m.

Notice that in this project we aimed at comparing surface waves recorded with DAS respect to standard surface waves of Rayleigh type that are recorded with vertical component geophones. Vertical component geophones are the ones commonly utilized in conventional MASW surveys. Horizontal component geophones which enable recording surface waves of Love types are not considered in this study.

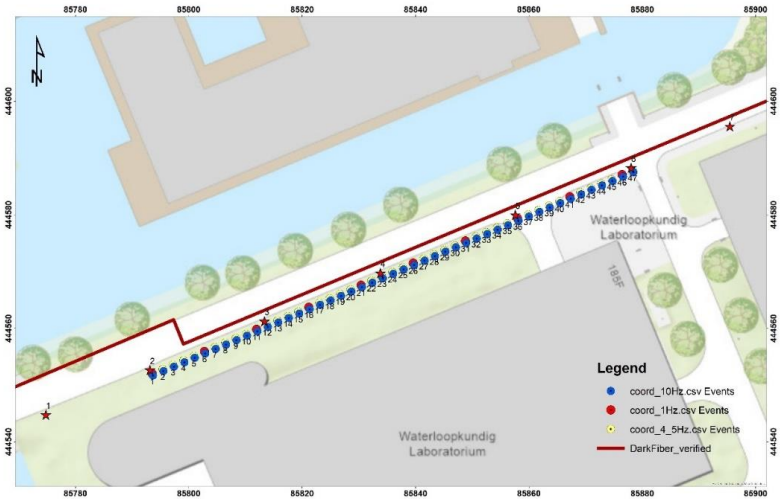

Figure 3.3 Geophone spreads and hammer blow impacts for active test (marked by red stars). For active MASW we use shot position 1, and for cross-correlation we use receiver 1 as the source receiver.

The selected 7 shot positions would be used to compute P-wave velocity tomography (10 Hz geophones), while the shot 1 (left most star in Figure 3.3) (18 m from the geophone spread to avoid clipping and near field effect problems) will be used to perform the active surface wave analysis (4.5 Hz geophones).

Table 3.2 DAS recording configuration. SR=Spatial Resolution, OD=Output Decimation, TD=Temporal Decimation, and P= Pulse width.

Parameter	Value	Remarks
SR or dx [m]	1.0	90 m of fibre parallel to the geophone spreads
OD	2x	To ensure P/OD ~ Gauge length/2
TD [s]	16	Highest sampling frequency = 16000 Hz
P	10	Optimum Pulse width
Duration [s]	30	Recording in continue mode
Gauge length [m]	10	Optimum for seismic applications

The DAS recording configuration implemented in this project is provided in Table 3.2. This configuration allows retrieving ambient noise data from all surrounding sources of high and low frequency. Figure 3.4 shows the active source and recoding systems utilized in the project. For the geophone spreads we used a GEODE seismograph manufactured by Geometrics that uses a *.seg2 data format and the DAS systems is an iDAS vr2, manufactured by Silixa uses the standard *.tdms format. The tdms DAS data are stored in an 8Tb external disk.

Figure 3.4 a) Vertical impactor, b) Geophone acquisition system, and c) iDAS interrogator for DAS measurements.

4 Data processing

4.1 Database preparation

Before the analysis started the recorded data needs to be stored in common data format compatible with the processing python library selected. During the acquisition the (continuous) data was saved using 15 seconds (GEODE) and 30 seconds (iDAS) time duration. The recorded data was re-arranged in 1.0-hour segments and saved in *.sac format, so the stored signals can be easily pre-processed with Obspy and later processed with NoisePy Package. For writing all traces in *.sac format we used the format writing functions provided by Obspy library.

An example on one of the signals saved in *.sac format is displayed in Figure 4.1. For each system all records are saved individually per trace, so every 1-hour folder contains all individual geophone and DAS traces. For this project we processed up to 170 hours of ambient noise records per systems.

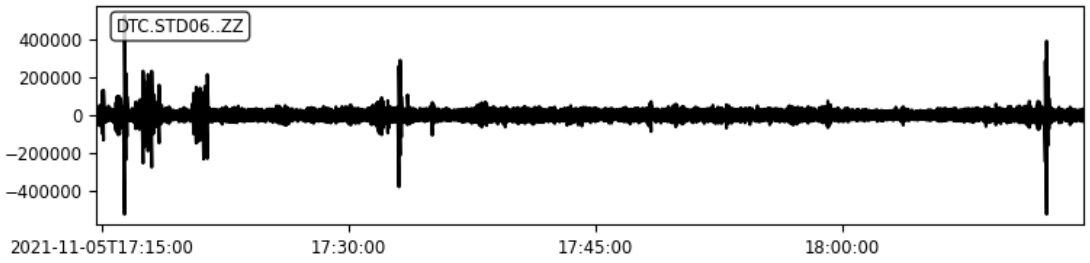

Figure 4.1 Example of 1-hour single trace noise record in sac format.

4.2 Surface wave passive processing

In this section we describe the processing scheme implemented. The seismic processing of the recorded ambient noise data consists of seismic interferometry analysis (described in section 2.1) aimed at computing virtual shot-gathers along the test site and selected fibre optic segments. The procedure is implemented utilizing the well-known open source codes: NoisePy (https://github.com/mdenolle/NoisePy) which is based on the Obspy (https://docs.obspy.org/) processing library. The computed virtual shotgathers are used to compute the phase velocity spectra (extraction of dispersion curve) which comprises the dispersion analysis. Finally, the retrieved dispersion curves are used to compute, via inversion, the S-wave velocity profiles underneath the receiver spread.

The processing scheme adopted in this project, is as follows:

a) Record selection and pre-processing along 60 s window:

- Selection of DAS traces along 90 m segments.

- Mean removal and signal detrend.
- Band-pass filtering [0.1 Hz - 100 Hz].

b) Interferometry:

- Time domain normalization. RMA (Running-Mean Average) normalization to enhance SNR.
- Frequency domain normalization. Spectral whitening.
- Cross-correlation.
- Band - Filtering of cross-correlated signals [1.0 Hz - 30 Hz].
- Linear and phase averaging of cross-correlated signals along several hours.

d) Dispersion analysis and inversion:

- Phase velocity spectrum computation (MASW) for individual 1-hour time segment.
- Dispersion curve extraction.
- Fundamental mode inversion using least-square method of SeisImagerSW software (SeisImager/SW - Geometrics : Geometrics).
- Velocity profile with the lowest misfit.

4.3 Surface wave active processing

The active surface wave processing is implemented following the criteria described in section 2.2 of the method section. At the test site active MASW were collected utilizing both a sledgehammer and/or a vertical impactor localized at 18 m from both ends (20% of the spread length) of the 90 m spread length (47, 4.5 Hz vertical geophones). The computed active phase velocity spectrum is used to extract the dispersion curve which is later inverted to compute the S-wave velocity profile. The active survey should provide information on the velocity structure at a maximum depth of 30 m.

The inverted S-wave velocity profile, from the active processing, will be later compared to the S-wave velocity profile computed from the passive surface waves analysis.

4.4 Shallow P-wave velocity structure

We perform the traditional P-wave refraction seismic survey (using 10 Hz geophones), as an aid to interprete the inverted S-wave velocity profile obtained via active and passive surface wave processing. For this, we assume that the P-wave velocity profile depicts similar velocity transitions (in depth) to the slower S-wave velocity obtained via surface wave inversion. For simplicity the refraction seismic method is not described in the method section, but the reader can refer to the classic bibliography about seismic exploration focused in refraction seismic surveying (Palmer, 1980; Redpath, 1973).

The retrieved P-wave 2D cross-section will be useful to correlate velocity changes (in depth) that may be observed in the 1D S-wave velocity profiles from either active and passive surface wave analysis. The P-wave velocity tomography is performed by inverting the measured travel-times utilizing an open source python-based library pygimli (https://www.pygimli.org/).

4.4.1 P-waves arrivals from passive dark fibre DAS data

We also performed noise cross-correlation from passive dark fibre data as implemented in section 4.2, but in higher frequency range [5.0 – 25 Hz]. The aim is to evaluate the possibility of retrieving first arrivals (direct waves) from the computed virtual shot-gathers, like the ones retrieved with the 10 Hz receivers generated by hammer impacts. The analysis will be focused on comparing the measured travel times with both systems. A more advanced body wave processing of the passive dark fibre data should be possible in a follow-up project.

5 Results

5.1 S-wave velocity profiling

5.1.1 Seismic interferometry – Geophone data

We initially present the results obtained with the reference geophone data, so we know, beforehand, the expected dispersion characteristics and the actual soil conditions of the soil at the test site location. The cross-correlation function (CCF) computed from 1.0 Hz geophones during 7 days of ambient passive noise data is presented in Figure 5.1. We observe that the CCF depicts coherent pulse-like waveforms for both the positive and negative time lags. The associated average phase velocity spectrum shows recovered coherent low frequency energy between 2.5 Hz - 4.5 Hz frequency range with propagating phase velocities varying between 100 m/s – 400 m/s.

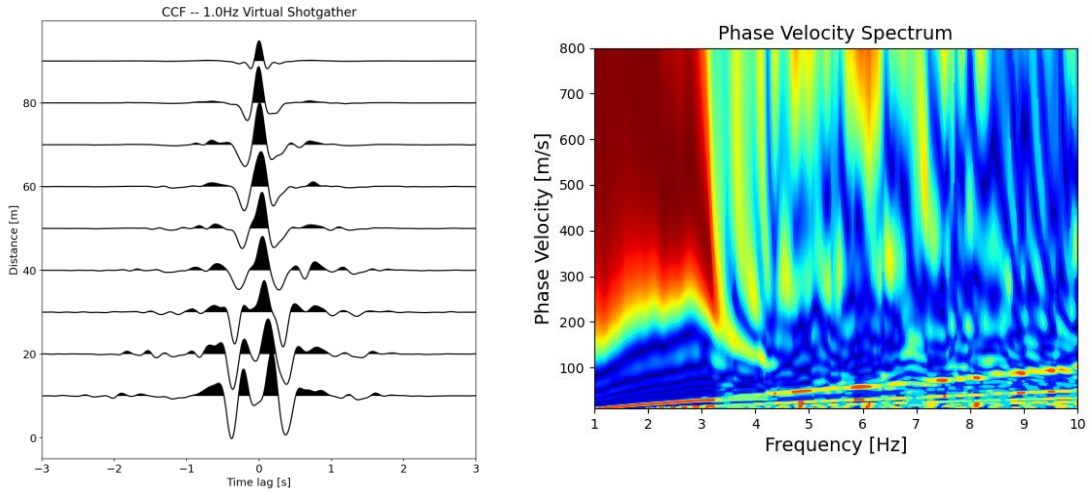

Figure 5.1 Cross-correlated function (left) and associated phase velocity spectrum (right) for 1.0 Hz geophone data. The linear patterns at the low phase velocity part is due to spatial aliasing.

Likewise, the 4.5 Hz noise data displayed in Figure 5.2 shows a rather consistent pattern in a similar frequency and phase velocity range as the 1.0 Hz geophones. However, the shorter receiver spacing enhances some energy patterns at frequencies up to 7.0 Hz. There is also pattern of a bit higher phase velocity, probably, related to higher mode energy.

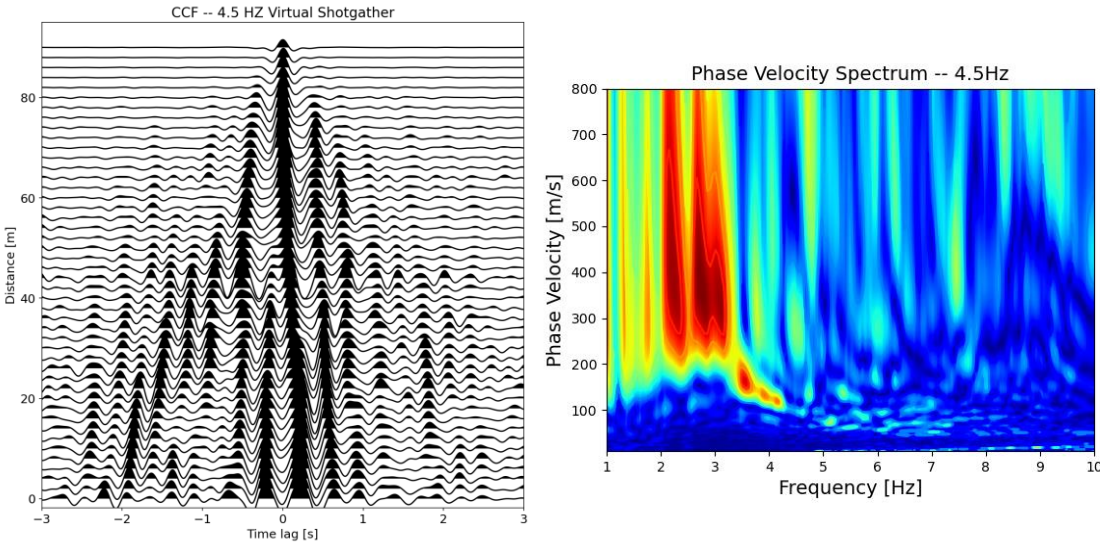

Figure 5.2 Cross-correlated function (left) and associated phase velocity spectrum (right) for 4.5 Hz geophone data.

5.1.2 Seismic interometry – DAS data

First, we discuss the frequency content of the recorded wavefield with all the measuring sensors. We present a comparative plot of the power spectral density function of DAS (for continuous 24 hours) with respect to standard 1.0 Hz and 4.5 Hz geophones in the 0.01 Hz – 100 Hz frequency range (Figure 5.3). At the high frequency part (25 Hz or higher), we observe that all systems recorded coherent noise generated by a vibrating container nearby at frequencies of 25 Hz, 50 Hz, and 75 Hz. At the low frequency part (below 25 Hz), the 1.0 Hz geophones depict a similar behavior to DAS, while for the 4.5 Hz geophone, as expected, the amplitudes start to decrease almost linearly below its resonance frequency.

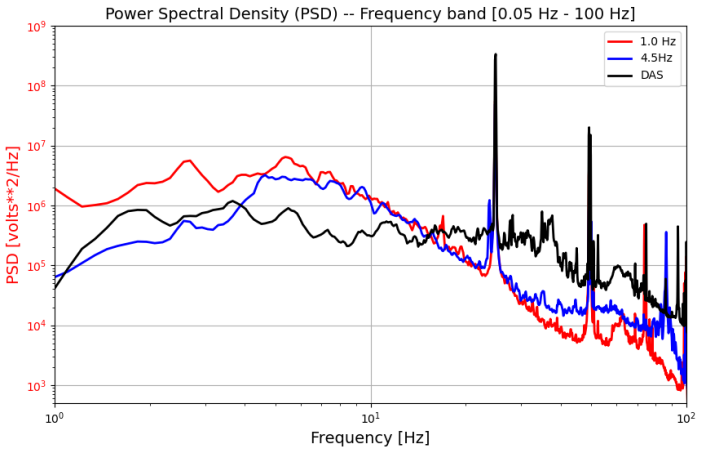

Figure 5.3 Average PSD for DAS respect to standard 1.0 Hz and 4.5 Hz geophones. PSD for continuous 24 hours. Note that the PSD are scaled down to match the amplitudes of the 1.0 Hz and 10.0 Hz receivers.

Before proceeding with the detailed analysis of the Dark fibre data, it is important to mention that from the 116 m of fibre available at the site, after cross-correlation, traces at coordinates 10 m – 29 m, showed inconsistent waveforms (Figure 5.4). This inconsistency, most likely, is caused by a lack of proper coupling between the fibre and surrounding soil. From 0 m – 10 m we still see continuity respect to traces at coordinates 29 m - 116 m. The lack of good coupling causes incoherent waveforms and time-delay with respect to the source-receiver, so the actual virtual shot gather cannot be successfully reconstructed for the full 116 m straight segment available. Therefore, for our analysis we utilized coordinates 29 m – 116 m (distance range), providing maximum length of 86 m.

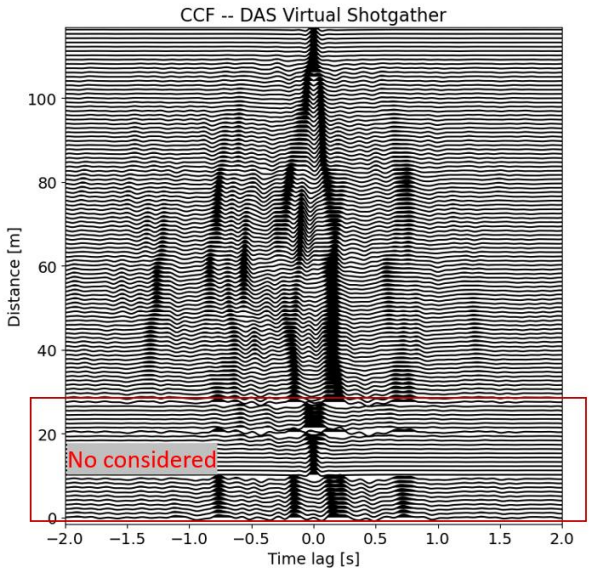

Figure 5.4 Computed CCF for 116 m straight segment. For our analysis only traces 29 to 116 are considered.

After carrying out cross-correlation along 1.0-hour continuous noise data, the computed CCF's show very coherent low frequency waveforms. An example of one of the computed CCF is displayed in Figure 5.5. The computed waveforms shows energetic wave patterns at both positive and negative time lags. The CCF's and associated phase velocity spectrum are computed from recorded at high (Figure 5.5a) and low (Figure 5.5b) noise levels. At high noise levels the phase velocity spectrum displays very energetic and consistent dispersive trend in a similar frequency and phase velocity range as shown in the reference geophone data displayed in Figure 5.1 and Figure 5.2. At low noise level, a consistent dispersion curve (incoherent behavior of phase velocity) cannot be determined, so the record could not be used for further analysis. A more detailed analysis of the time variation of the phase velocity spectra is presented in the coming section.

The coherent dispersion pattern provided information in between 2.5 Hz and 4.5 Hz for a wavelength range between 40 m - 90 m which gives a minimum and maximum exploration depth of 13 m and 30 m respectively.

a)

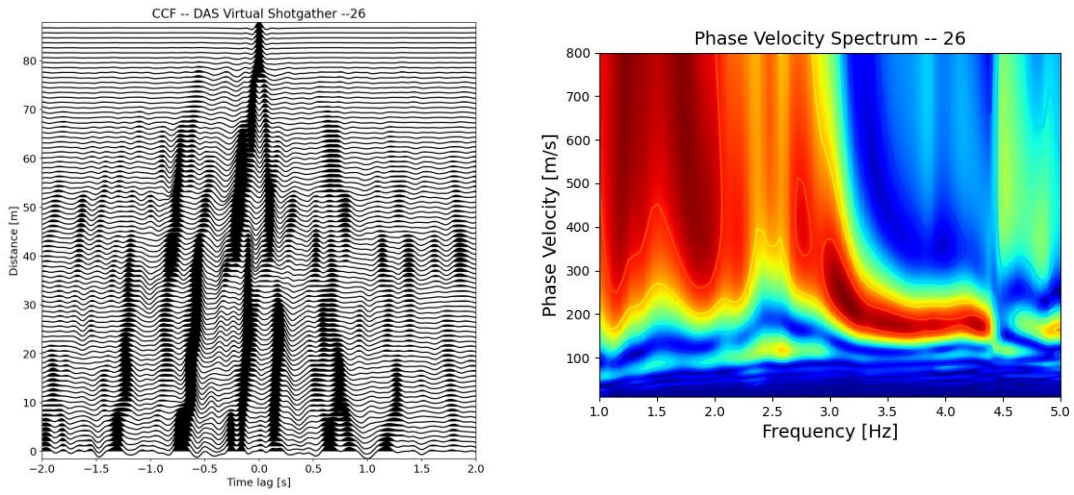

b)

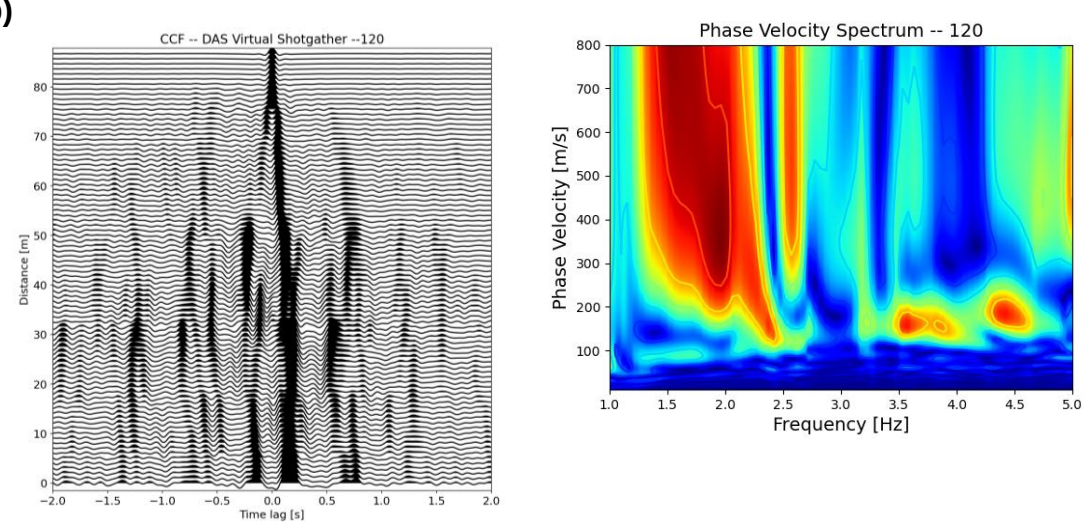

Figure 5.5 Cross-correlated function from DAS data for a) coherent and b) incoherent phase velocity spectrum.

As shown in Figure 5.5 the ambient noise data not always exhibit a coherent and energetic phase velocity spectrum. The temporal variation of the phase velocity spectrum is displayed in Figure 5.6. It is observed that the phase velocity distribution varies with time with a marked difference between those hours with higher and lower traffic activity. Specifically, the coherent and constant phase velocity in the 150 m/s – 350 m/s appears more energetic around 12:00 – 17:00 hours which is the time with more running traffic. On the other hand, the lowest energy occurs during the evening between 18:00 – 6:00 which are the hours with the lowest (to almost no) running traffic. Some of the individual phase velocity spectrum for various ambient noise conditions (utilized to construct Figure 5.6) recorded during the 7 days for 1-hour interval are displayed in Appendix C. The phase velocity distribution over time can be used to select those time segments where the phase velocity appears with the lowest signal-to-noise ratio, and hence a more accurate Vs profile can be computed.

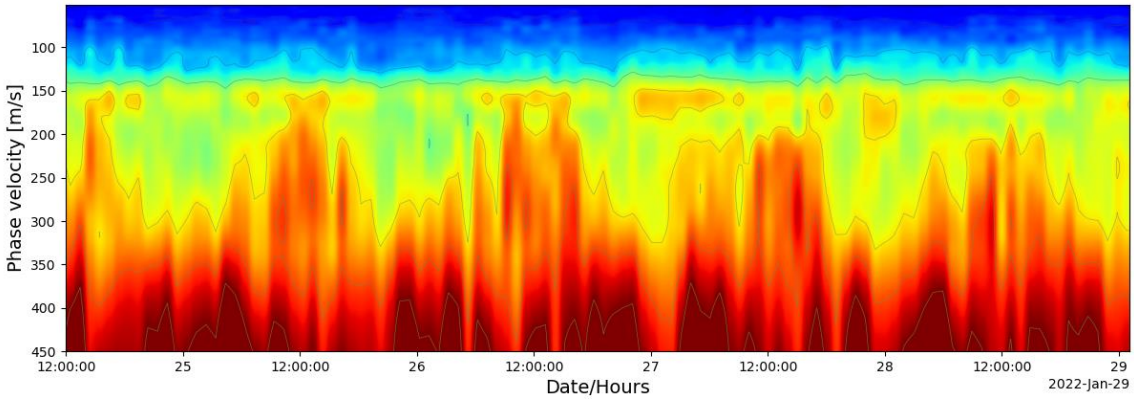

Figure 5.6 Temporal distribution of the computed phase velocity. Phase velocity spectra are averaged over frequency per hour. Phase velocity are non-normalized.

5.1.3 Computed S-wave velocity profiles

Dispersion curves retrieved from the maximum amplitudes of the energetic pattern are utilized to compute S-wave velocity profiles. In Figure 5.7 we show the average DAS phase velocity spectrum (30 best phase velocity spectra at the highest traffic hours defined in Figure 5.6), black and white background color, with the extracted dispersion curve delineated by the peak amplitude energy (red line). On top of the phase velocity spectrum there are the dispersion curves from the 4.5 Hz, 1.0 Hz, and 4.5 Hz (Sledgehammer impacts), see Appendix A. The dispersion curves of the geophone data were computed from average phase velocity spectrum computed from those individual spectra with the most coherent dispersion patterns, so from 170 hours of data we selected the best 30 hours of phase velocity spectra. We also include the phase velocity spectrum computed from active hammer blows. The average phase velocity spectra computed from geophone data are displayed in appendix D.

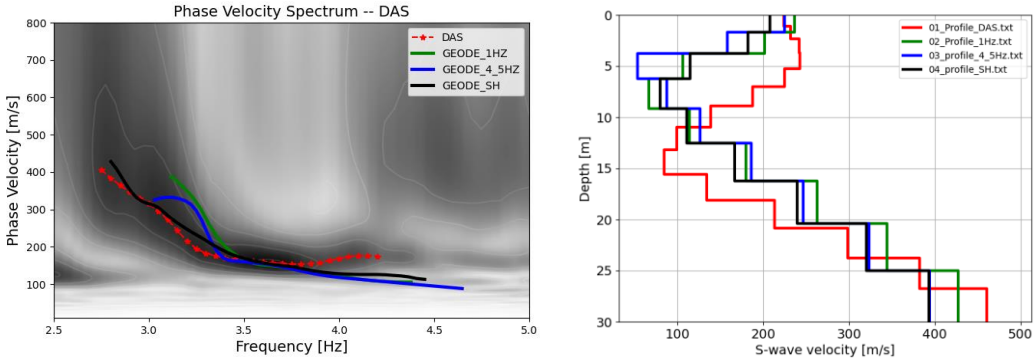

Figure 5.7 Measured dispersion curves (left) and inverted S-wave profiles (right).

Overall, the 4 inverted S-wave profiles show a similar behavior with a decremental behavior in velocity from 200 m/s down to 100 m/s which later increases gradually up to 400 m/s (Figure 5.7). Regarding the depth transitions, the geophone data show very similar transitions with the low velocity layer (~ 100 m/s or less) in a depth range of 7 m – 12 m depth, while the DAS shows a deeper transition between 11 m - 16 m depth. The average Vs30 values out of the 3 reference profiles is about 168 m/s which is about 10% slower than the Vs30 value (187 m/s) obtained with the DAS profile.

5.2 P-wave velocity

5.2.1 P-wave tomography – Active reference data

In this section we analyze the potential of DAS to retrieve the first break that can provide P-wave velocity at the site. The analysis is focused on the similarities between travel times recorded with DAS with respect to the ones recorded with 10 Hz geophones. The recorded 10 Hz reference data consists of active body wave data generated with the vertical impactor. An example of a refraction seismic record is shown in Figure 5.8 where clear P-wave first arrivals are observed. The travel times from had picked first arrivals (see appendix B) are utilized to compute 2D P-wave tomography at the site, as an aid to assess potential implications of the actual 2D layering in the measured surface waves.

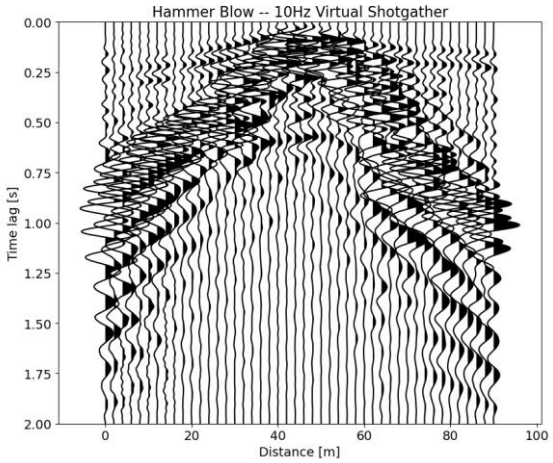

Figure 5.8 Active refraction seismic record using 10.0 Hz vertical geophones.

The inverted 2D Vp tomography image (Figure 5.9) provides the main velocity distribution revealing a marked non-horizontal layering at first 30 m depth, with a sharp lateral velocity transition between coordinates 20 – 40 m. It is observed that at the left-side (0 – 30 m) of the profile the stiff formation of 1200 m/s or higher appears shallower, while at the right side (30 m – 100 m) there is a more uniform and softer layer of 20 – 25 m thickness overlaying the 1200 m/s or higher velocity formation.

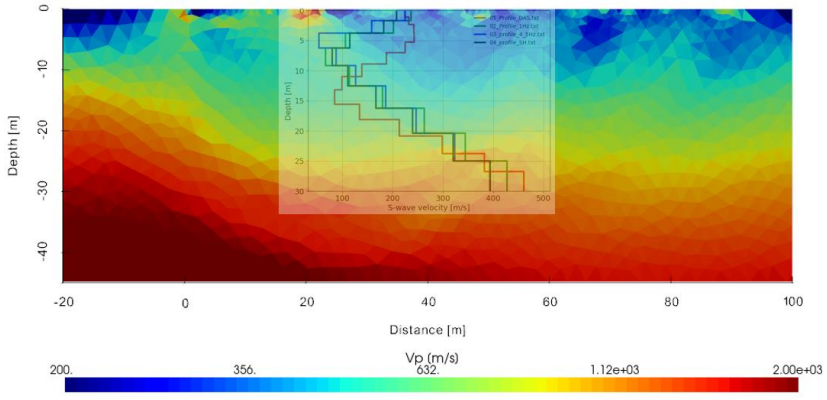

Figure 5.9 Vp tomography under the selected test segment together with the inverted 1D S-wave profiles.

5.2.2 P-wave arrivals from DAS-CCF

We processed the ambient noise data for body wave BW processing using 10 Hz geophones and DAS data. Before computing CCF, the data was band-pass filtered in 5.0 Hz – 25.0 Hz frequency range. Figure 5.10 shows asymmetric wave propagation along the selected traces, which may be caused by the marked lateral variation and the asymmetric nature of the incoming surrounding sources. The computed CCF with the 10 Hz receivers shows a prominent wave pattern in the positive lags [0.0 s – 0.8 s] between traces 44 to 90; which is not captured with the DAS system. In the DAS CCF there is a coherent high velocity trend bounded by the first 0.25 s between coordinates 43 – 82. This pattern seems to be also present in the 10 Hz data.

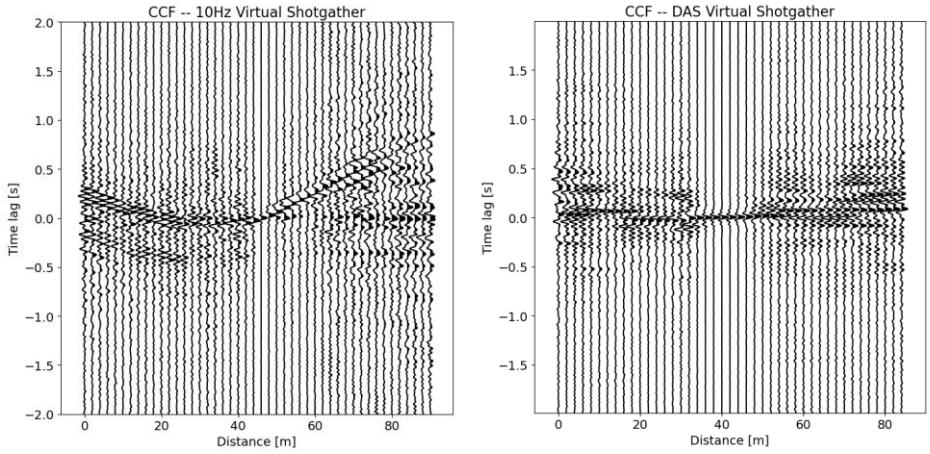

Figure 5.10 Computed cross-correlation functions for 10 Hz and DAS systems along the test line. Both CCF are computed from 170 hours of continuous noise data.

Now, we compare a selected DAS time window and plot it together to an individual shotgather with 10 Hz receiver spread (for both, hammer blow and passive). We analyze the similarities between the P-wave velocity associated travel times or first arrivals with both systems. Figure 5.11 shows the selected traces from coordinates 46 m to 90 m for the 10 Hz array and coordinates from 43 m to 96 m for DAS.

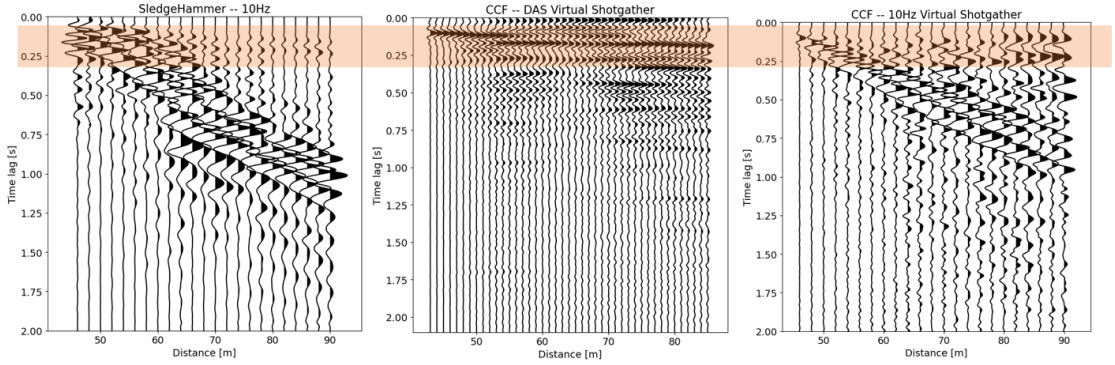

Figure 5.11 Selected time domain segment for an individual shot record with 10 Hz geophones (left), cross-correlation function for DAS (middle), and 10 Hz CCF (right).

We highlight the most prominent first arrivals and from there analyze if the computed DAS wave forms are comparable to the traditional system. Note that in the CCF-DAS virtual shotgather surface wave appears to be suppressed, mainly because surface waves at the site are dominant in

the 2.0 – 5.0 Hz range while the this was correlated in the 5.0 Hz – 25.0 Hz frequency range. It is also observed that the 10 Hz CCF shows coherent first arrivals between 80 – 90 m.

In Figure 5.12 we plot the extracted travel times from interpreted first breaks from the 2 systems. The retrieved DAS travel times seems to match well at the first few traces (x<55 m), but later diverge (x>55 m) from the reference 10 Hz receiver spread.

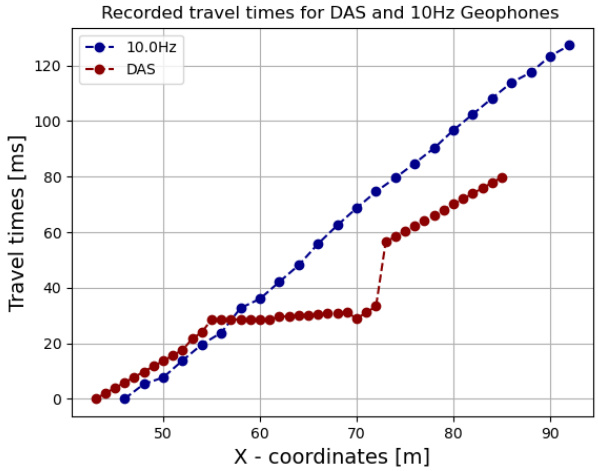

Figure 5.12 Computed travel times using Hammer blows and CCF at the middle of the array. The 10Hz travel times correspond to the average values computed from 5 individual shots at the middle of the array, while the CCF – DAS is computed from the average waveforms after stacking 170 hours of noise data.

5.3 DAS sledgehammer test results

During the refraction seismic survey, we utilized the vertical impactor to get energy enough to illuminate the whole 90 m receiver spread. However, the vertical impactor generated just too much energy that the Dark fibre signals were clipped. Therefore, we performed an additional sledgehammer tests (using a 8 kg sledgehammer) to assess the potential of the dark fibre utilized to pick up coherent body and surface wave energy.

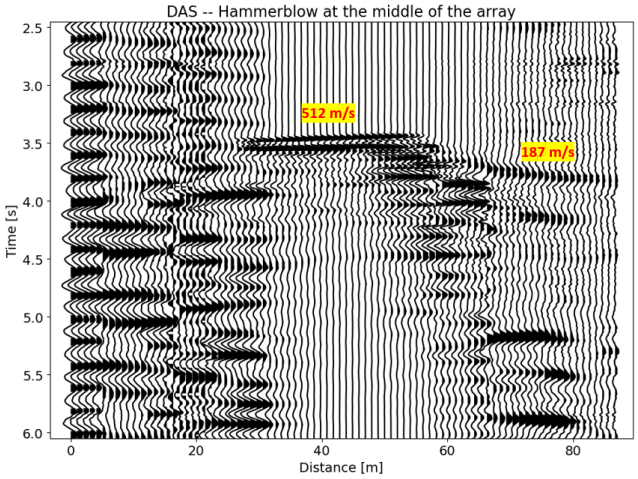

Figure 5.13 DAS - Dark Fibre sledgehammer record. On top there is the estimated apparent P-wave velocity.

Figure 5.13 shows the wave trends recorded after a hammer impact around the middle position of the dark fibre segment. The computed velocities at the left and right side of the array appears in agreement with the velocities determined in the Vp tomography in Figure 5.9. Figure 5.14 shows the phase velocity spectrum utilizing the first 48 traces of the active dark fibre shot recorded displayed in Figure 5.13. Clearly, the dark fibre record from sledgehammer impact retrieves surface wave energy that can be utilized to retrieve the shallow S-wave velocity structure.

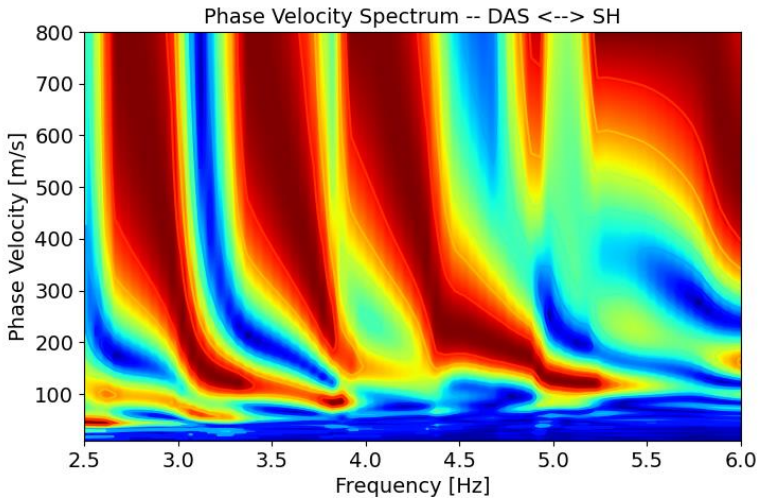

Figure 5.14 Phase velocity spectrum computed from an active Dark fibre record.

6 Discussion

The computed DAS cross-correlation functions reveal the potential of the selected Dark Fibre for shallow ground characterization in terms of S-wave velocity. Despite the overall velocity distribution of the computed velocity profiles between DAS and the geophone data are rather similar, the actual low velocity transition does not occur at the same depth range. These discrepancies may be related to a combination of factors, such as position of the selected fibre with respect to the position of the lateral variation observed in the P-wave tomography (offset of ~7.0 m), the uni-directional sensitivity nature of the fibre, and variations in the coupling conditions of the fibre.

In our selected fibre there was 116 m of straight fibre available. However, from coordinates 10 m to 30 m the fibre depicted poor or incoherent waveforms indicating poor coupling conditions in that specific segment. Although, this 20 m gap of data prevented us to increase the depth of exploration at the site, the selected segment provided enough coverage comparable to the geophone spreads.

The first arrivals derived from DAS appear to show very poor correlation with 10 Hz geophones. However, the processing performed here was rather simplistic, so better results may be obtained if using more advanced processing techniques to analyze not only the first-breaks but also the reflected P-waves which are of interest for reflection seismic exploration.

The results presented here demonstrate the great potential of dark fibre for shallow surface characterization, and it is in line with the findings reported in the literature. For geothermal applications, the implementation of Dark fibre will require to scale it up to the kilometer scale; thus, the array aperture is at least 3 times the target depth. This will enable the possibility of investigating very deep S-wave velocity structure specially in urban areas where deploying standard sensors is virtually impossible. However, the uncertainties regarding the state the fibre, exact location or geometry of the fibre (whether is fully horizontal or not) and coupling conditions must be further investigated. The geometry of the dark fibre will poses an enormous challenging, because there is basically no way to verify the geometry with very high accuracy. On the other hand, the state of the fibre and the coupling conditions could be assessed by performing a monitoring campaign, so the quality of the whole dark fibre selected can be evaluated in time (signal amplitudes at day and night) and frequency domain (frequency content at day and night). This monitoring scheme would require automatizing of the processing, so the segments of poor quality can be discarded.

7 Conclusions

After discussing the results of this research, we define the following conclusions:

- The results obtained in this project indicate that Dark Fibre certainly retrieves coherent and consistent ambient noise (traffic noise) that can be successfully used for seismic interferometry.

- The lack of good coupling of the fibre with the surrounding soil can affect the quality of the cross-correlation signals preventing signal continuity with respect to the source-receiver as observed in the initial part of the selected fibre optic cable.

- The quality of the phase velocity spectrum appears to vary with time depending on the level of the nearby traffic, so for subsequent dispersion analysis the average phase velocity spectrum should be computed using selected times with high traffic activity.

- The overall S-wave velocity of the computed DAS profile appears in good agreement with the layer distribution computed by the standard geophone (Average difference of the Vs30 at the site is of 11%). The computed profile appears to match the actual transitions at the test line. Despite the similarities observed between DAS and geophones data, there is a possibility that a better match could have been obtained if using horizontal geophones. This topic, however, should be further investigated in a follow up project.

- The first assessment on the potential of dark fibre for passive P-wave profiling (active P-wave should work) showed a rather poor agreement between the observed first breaks with the DAS signals with respect to the standard systems. However, the first results should not be considered conclusive, due to the simplistic nature of the approach adopted for the assessment, so more advanced processing could improve the presented results.

- The processing scheme utilized here can be implemented in kilometer scale array, so deep S-wave velocity profiles can be computed in areas with induced seismicity related to geothermal well production. This is especially beneficial in urban areas where there is almost no space to place large aperture standard survey systems.

8 Acknowledgements

We want to acknowledge the joint effort by WarmingUp initiative and Deltares that enabled the possibility of gaining new knowledge on the potential of existing fibre optic cables as seismic sensors. We want to thank the great contribution by PierPaolo Marchesini and Athena Chalari from Silixa who assisted us in setting up the fibre optic acquisition parameters. We also acknowledge the valuable comments and suggestions provided by Bob Paap from TNO and Guy Drijkoningen from TUDelft who helped to further improve this report. Finally, we want to value the great contribution by our colleagues Edvard Ahlrichs who assisted us in the field deployment and Paul Vlenterie who guided us on the use and selection of the spare fibre at Deltares campus in Delft.

9 References

Ajo-Franklin, J. B., Dou, S., Lindsey, N. J., Monga, I., Tracy, C., Robertson, M., . . . Daley, T. J. S. r. (2019). Distributed acoustic sensing using dark fiber for near-surface characterization and broadband seismic event detection. *9*(1), 1-14.

Bensen, G., Ritzwoller, M., Barmin, M., Levshin, A. L., Lin, F., Moschetti, M., . . . Yang, Y. (2007). Processing seismic ambient noise data to obtain reliable broad-band surface wave dispersion measurements. *J Geophysical Journal International, 169*(3), 1239-1260.

Daley, T. M., Freifeld, B. M., Ajo-Franklin, J., Dou, S., Pevzner, R., Shulakova, V., . . . Henninges, J. J. T. L. E. (2013). Field testing of fiber-optic distributed acoustic sensing (DAS) for subsurface seismic monitoring. *32*(6), 699-706.

Dou, S., Lindsey, N., Wagner, A. M., Daley, T. M., Freifeld, B., Robertson, M., . . . Ajo-Franklin, J. B. J. S. r. (2017). Distributed acoustic sensing for seismic monitoring of the near surface: A traffic-noise interferometry case study. *7*(1), 1-12.

Foti, S., Hollender, F., Garofalo, F., Albarello, D., Asten, M., Bard, P.-Y., . . . Socco, V. (2018). Guidelines for the good practice of surface wave analysis: a product of the InterPACIFIC project. *Bulletin of Earthquake Engineering, 16*(6), 2367-2420. doi:10.1007/s10518-017-0206-7

Gabriels, P., Snieder, R., & Nolet, G. (1987). In situ measurements of shear-wave velocity in sediments with higher-mode Rayleigh waves. *J Geophysical prospecting, 35*(2), 187-196.

Garofalo, F., Foti, S., Hollender, F., Bard, P., Cornou, C., Cox, B. R., . . . Di Giulio, G. (2016). InterPACIFIC project: Comparison of invasive and non-invasive methods for seismic site characterization. Part I: Intra-comparison of surface wave methods. *J Soil Dynamics Earthquake Engineering, 82*, 222-240.

Kruiver, P. P., van Dedem, E., Romijn, R., de Lange, G., Korff, M., Stafleu, J., . . . van Elk, J. J. B. o. E. E. (2017). An integrated shear-wave velocity model for the Groningen gas field, The Netherlands. *15*(9), 3555-3580.

Lellouch, A., Spica, Z., Biondi, B., & Ellsworth, W. (2019). *Using vertical DAS arrays for continuous monitoring of induced seismicity.* Paper presented at the 81st EAGE Conference and Exhibition 2019 Workshop Programme.

McMechan, G. A., & Yedlin, M. J. (1981). Analysis of dispersive waves by wave field transformation. *J Geophysics, 46*(6), 869-874.

Palmer, D. (1980). *The generalized reciprocal method of seismic refraction interpretation*: Society of Exploration Geophysicists.

Park, C., Miller, R., Rydén, N., Xia, J., & Ivanov, J. (2005). Combined use of active and passive surface waves. *J Journal of Environmental Engineering Geophysics, 10*(3), 323-334.

Park, C. B., & Miller, R. D. (2008). Roadside passive multichannel analysis of surface waves (MASW). *J Journal of Environmental Engineering Geophysics, 13*(1), 1-11.

Park, C. B., Miller, R. D., & Xia, J. (1999). Multichannel analysis of surface waves. *J Geophysics, 64*(3), 800-808.

Redpath, B. B. (1973). *Seismic refraction exploration for engineering site investigations*. Retrieved from

Sambridge, M. (1999a). Geophysical inversion with a neighbourhood algorithm—I. Searching a parameter space. *Geophysical Journal International, 138*(2), 479-494. doi:10.1046/j.1365-246X.1999.00876.x %J Geophysical Journal International

Sambridge, M. (1999b). Geophysical inversion with a neighbourhood algorithm—II. Appraising the ensemble. *Geophysical Journal International, 138*(3), 727-746. doi:10.1046/j.1365-246x.1999.00900.x %J Geophysical Journal International

Tribaldos, V. R., Ajo-Franklin, J., Dou, S., Lindsey, N., Ulrich, C., Robertson, M., . . . Tracy, C. (2019). Surface Wave Imaging using Distributed Acoustic Sensing Deployed on Dark Fiber: Moving Beyond High Frequency Noise.

Wapenaar, K., & Fokkema, J. J. G. (2006). Green's function representations for seismic interferometry. *71*(4), SI33-SI46.

Wathelet, M. (2008). An improved neighborhood algorithm: parameter conditions and dynamic scaling. *J Geophysical Research Letters, 35*(9).

APPENDICES

Appendix A -- Inverted Profiles

In the plots below, black curves are the theoretical dispersion curve, and the green dots are the measured dispersion curves.

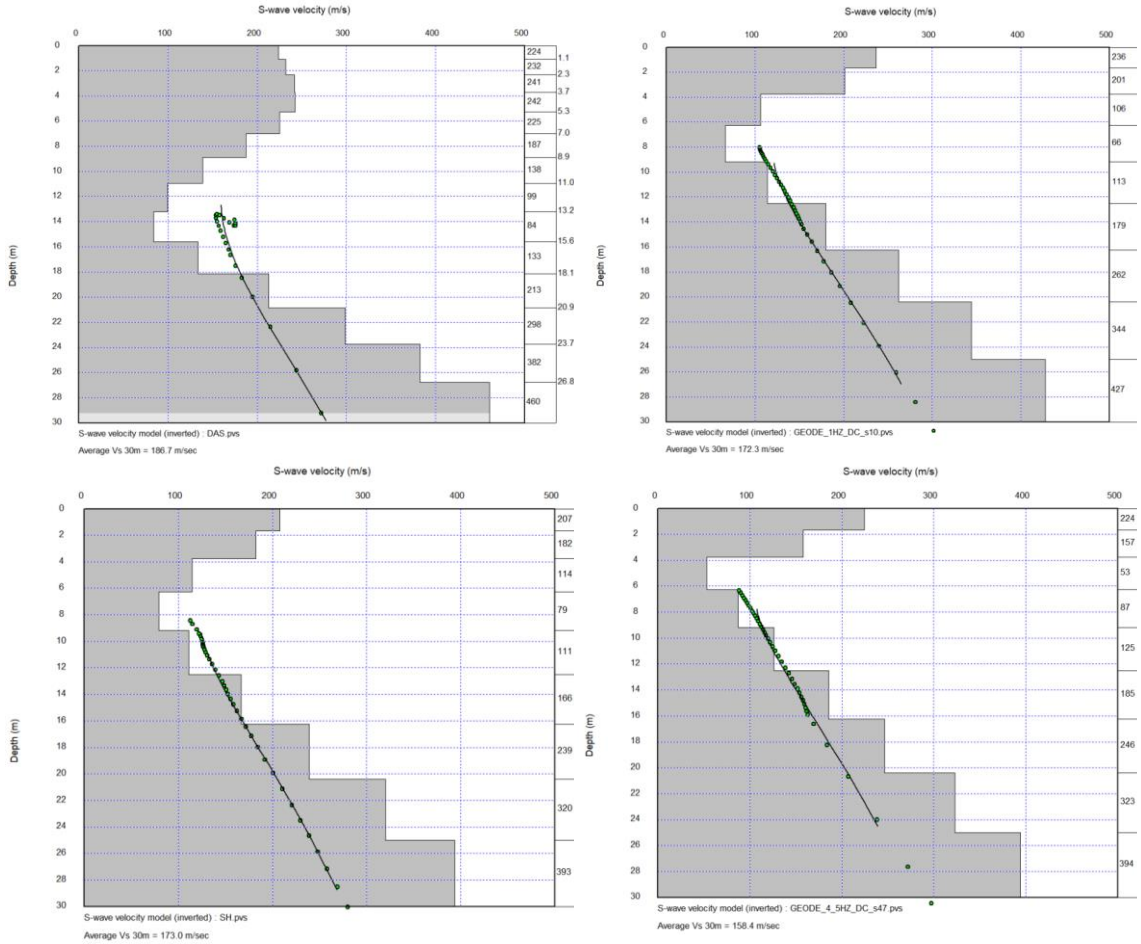

Appendix B – Travel times from 10 Hz refraction seismic survey

The dotted lines are the average hand-picked travel times from 5 shot positions.

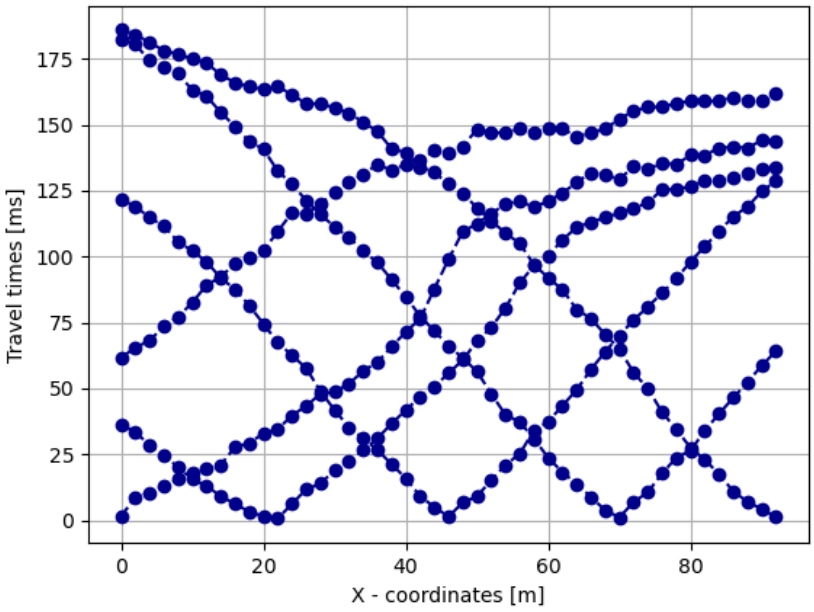

Appendix C – DAS Cross-correlation functions and phase velocity spectra

- **C-1: CCF**

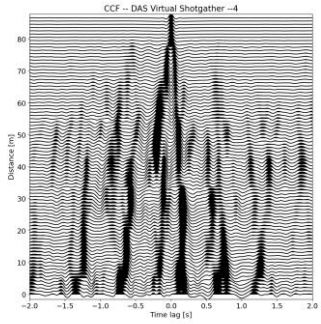

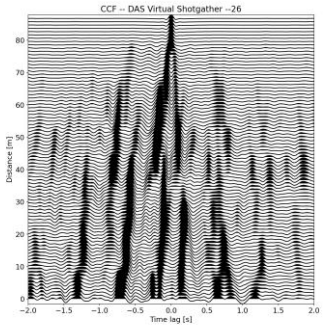

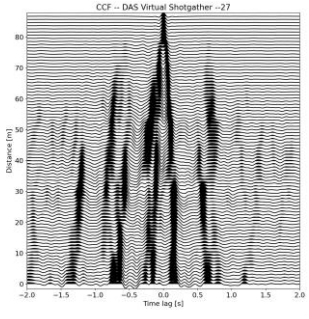

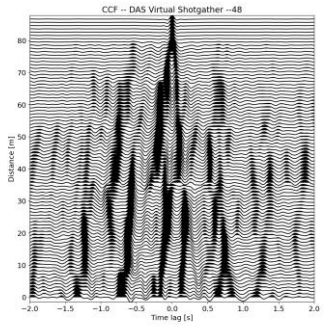

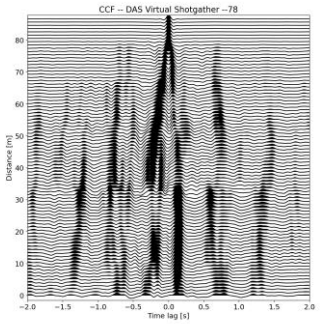

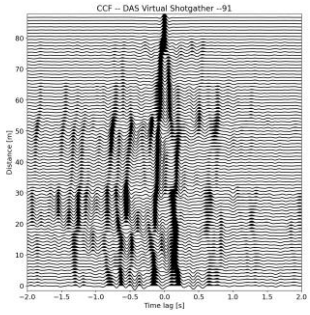

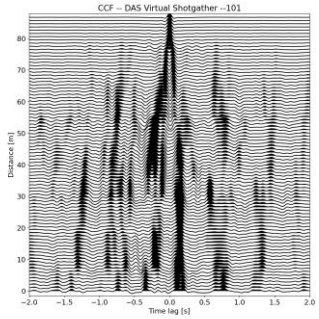

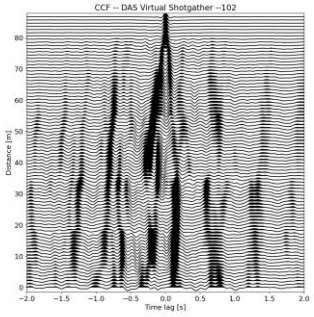

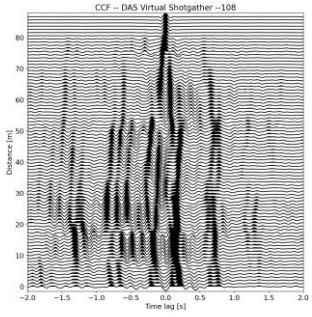

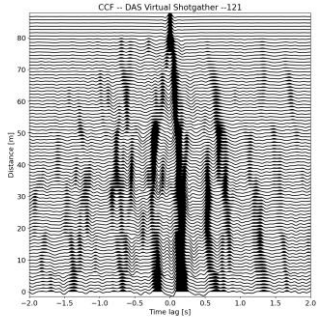

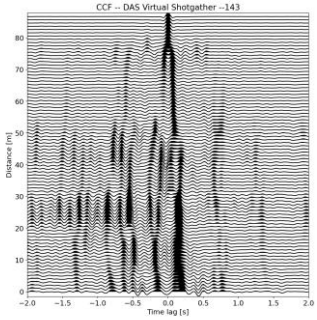

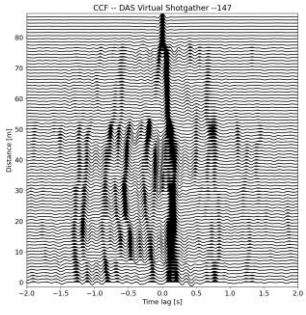

- **C -2: Phase velocity spectra**

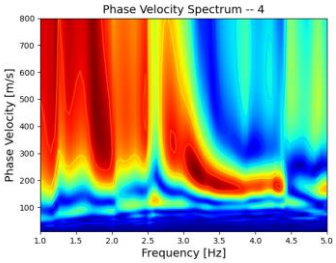

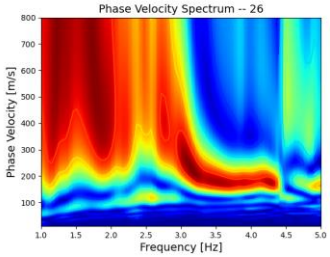

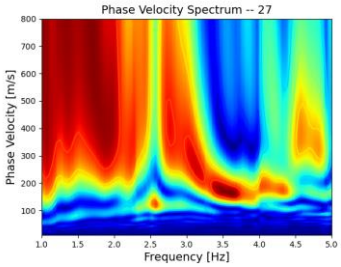

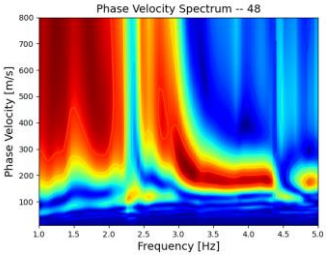

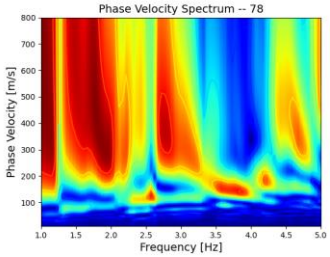

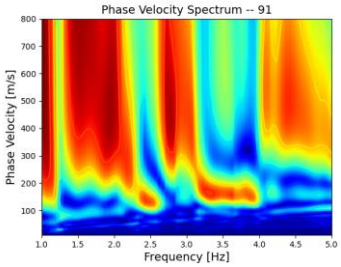

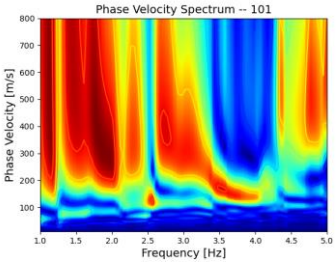

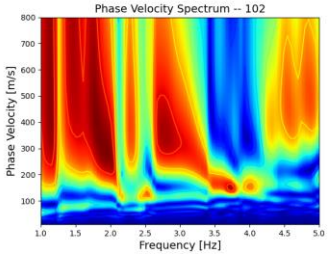

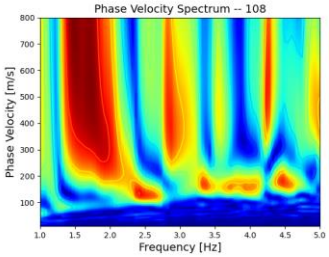

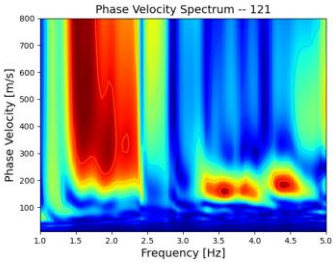

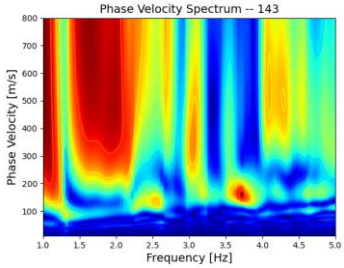

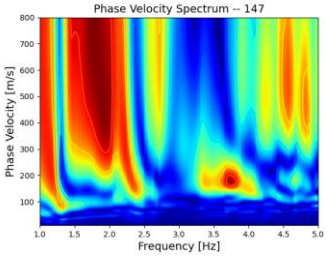

Appendix D – Average phase velocity spectra from geophone data

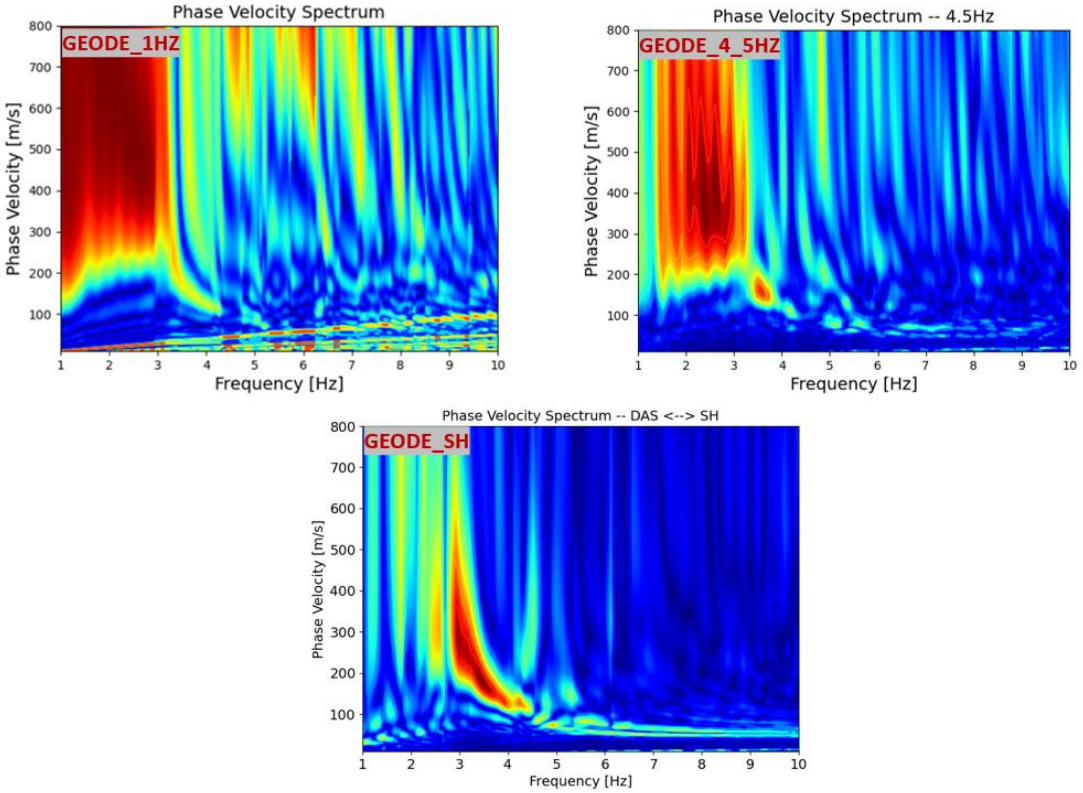

WARMINGUP
Innovatief Duurzaam Warmtecollectief

Adres
Princetonlaan 6
3584 CB Utrecht

Postadres
Postbus 80015
3508 TA Utrecht

Telefoon
088 866 42 56

E-mail
contact@warmingup.info

Website
www.warmingup.info

Version 6 **15 juni 2022**